



Stockholm  
University

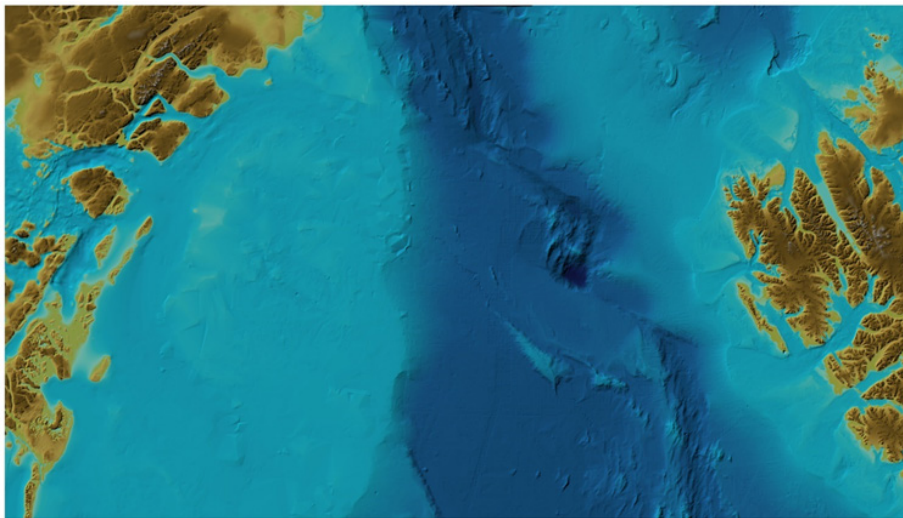
# Bachelor Thesis

Degree Project  
in Marine Geology 15 hp

## **The effects of gridding algorithms for compilation of bathymetric data**

A case study on data from the Fram Strait  
between Greenland and Svalbard

Linda Karlsson



Stockholm 2019

Department of Geological Sciences  
Stockholm University  
SE-106 91 Stockholm  
Sweden

## Abstract

The Fram Strait, located between Greenland and Svalbard, is the study area of this Bachelor Thesis. Its seafloor encompasses large depth variations and a great variety of undersea features and the bathymetric data coverage varies greatly across the selected study area. This makes the area excellent for studies of the effects of different gridding algorithms applied to compile a Digital Bathymetric Model (DBM). For this project, a bathymetric dataset was provided from the International Bathymetric Chart of the Arctic Ocean (IBCAO) database. Four different gridding algorithms were applied on this test dataset using three different software. Subsequent analyses to study the differences between the resulting DBMs were made. The cell sizes chosen were 100, 200, 250, 500, 1000 and 2000 m on a Polar Stereographic projection, which resulted in different degrees of preservation of the undersea features. Fledermaus was utilized to visualize the data without interpolations, and as an analyses tool where comparison between the data and the produced grids were made in the search of artifacts. GMT was used for gridding the data with the algorithms Surface Spline with Tension, Triangulation, and Block median. The Surface Spline with Tension created a great amount of spatial aliasing in areas where the bathymetry has short wavelengths and when gridding is made with small cell-sizes. Triangulation had to be done on subsets of the full data due to memory issues. These subsets were made as overlapping areas to ensure full coverage. Block median created a near artifact-free grid, but does not interpolate between soundings. Simple Kriging was done using SAGA tools in QGIS, though due to the size of the data file, this method could not be completed efficiently. For this reason it is concluded in this thesis that it is the least applicable algorithm for gridding large datasets. For data files of great variety and substantial size, it would be most efficient to use the Triangulation technique, as the great variety in data is not hampering the results of this method.

# Content

1. Introduction .....	5
2. Background .....	7
2.1 Geological setting .....	7
3. Material and Method .....	8
3.1 Python.....	8
3.2 Fledermaus .....	8
3.3 GMT .....	9
3.3.1 Surface Spline with Tension.....	9
3.3.2 Triangulation .....	9
3.3.3 Block median.....	10
3.4 SAGA Kriging.....	10
3.4.1 Simple Kriging .....	10
4. Results .....	10
4.1 Fledermaus .....	10
4.2 GMT .....	12
4.2.1 Surface Spline with Tension.....	12
4.2.2 Triangulation .....	13
4.2.3 Block median.....	14
4.3 SAGA Kriging.....	15
4.3.1 Simple Kriging .....	15
5. Discussion .....	15
5.1 Fledermaus .....	15
5.2 GMT .....	17
5.2.1 Surface Spline with Tension.....	17
5.2.2 Triangulation .....	18
5.2.3 Block median.....	19
5.3 SAGA Kriging.....	19
5.3.1 Simple Kriging .....	19
6. Conclusion.....	20
Acknowledgment.....	20
References .....	21
Appendix .....	22
1. Python.....	22
2. GMT .....	22
2.1 Surface.....	22

2.2 <i>Triangulate</i> .....	22
2.3 Block median.....	22
2.4 Source files .....	23

## 1. Introduction

The application of gridding to compile sparse data is common when portraying surfaces for a variety of different purposes (Weatherall et al., 2015). The gridding methods may vary, depending on purpose, the conditions of the data, and other variables, stemming from the fact that different algorithms will treat data differently and result in differences (e.g. Hell and Jakobsson, 2011; Smith and Wessel, 1990). To properly identify differences resulting from various algorithms utilized for gridding of data, it is necessary to use the same test dataset, to avoid questions where potential deviations originate from. In addition, to be able to observe how different algorithms are handling variations in quality and quantity of data when producing a regular gridded output (hereafter referred to as “grids”), a dataset of great variety is preferred. A bathymetric surface represented by a regular grid or Triangulated Irregular Network (TIN) is commonly referred to as a Digital Bathymetric Model (DBM) (Weatherall et al., 2015).

The study area chosen in this Bachelor Thesis, which agrees with the requirements of having areas of both rich and poor data coverage as well as areas of large variation in bathymetry, is the Fram Strait between Svalbard and Greenland (Fig. 1). The Fram Strait has areas that has been well traversed by vessels gathering data of the sort required for this project, and there are as well areas completely lacking data. Bathymetric data (depth soundings) from this area was provided from the updated International Bathymetric Chart of the Arctic Ocean (IBCAO) database (Jakobsson et al., 2012). This dataset was comprised of a great amalgamation of files, which originated from different sources and covered different extents (Fig. 2). The coverage of the data files does not create a full surface, as there are sections with no data collected. It is these empty areas, portrayed in white in Figure 2, that are the largest sections where interpolation is of a need for creation of a DBM.

The data from the area of interest (AOI) were gridded using four different approaches in three different software packages, to then compare the results, and judge which method of gridding were best suited for this type of dataset. This includes the TIN, even though this sometimes not is considered a proper “grid model”. The data was plotted in Fledermaus, where no interpolations were made, but rather only the extent of the data available in the file. In the software package GMT (Generic Mapping Tools), three gridding algorithms were used to try out which would present the best end result, i.e. the best preserved data, and the best representation of features (Wessel and Smith, 1991). The first two of these algorithms were *surface*, which creates a minimum curvature spline with tension, and *triangulate*, which applies a Delaunay triangulation of the depth data points to create a TIN (Triangulated Irregular Network) DBM. The third algorithm was *blockmedian*, which calculates the median depth value in a grid cell which then is used as input to a second run with *surface*. The fourth interpolation was done in the Open Source GIS software QGIS (version 3.4 Madeira), where SAGA (Open Source System for Automated Geoscientific Analyses) provides a *Simple Kriging* algorithm. These four different methods are here analyzed for their suitability to produce a DBM of the test dataset. Specifically, the analyses target if features may have disappeared or appeared and/or if artifacts have appeared from the actual gridding. By identifying the artifacts’ origins, the aptness of the combination of this type of dataset to a specific variety of module could be deciphered, and through this, the most appropriate method of gridding could be decided upon.

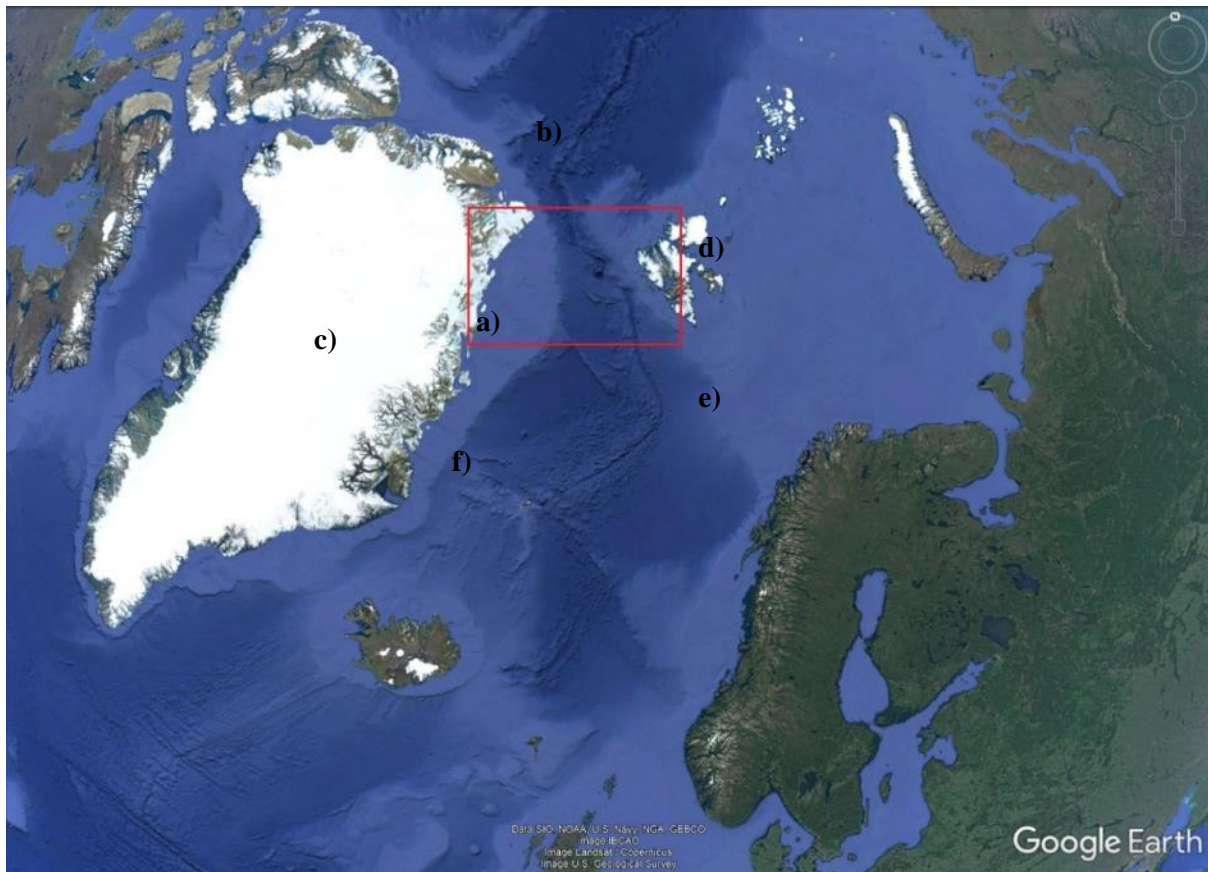


**Figure 1:** This map shows the a) area of interest (AOI) in the Fram Strait marked with a red square, in-between the features b) the Arctic Ocean in the north, c) Greenland in the west, d) Svalbard in the east, e) the Norwegian Sea in the southeast, and f) the Greenland Sea in the southwest.



**Figure 2:** Extraction from seabed.geo.su.se/ibcao, showing the individual data files that together comprises the dataset used for this project. The area is the AOI as marked by a) in Figure 1.

## 2. Background

### 2.1 Geological setting

An appropriate dataset, which fits the given criteria of consisting of different data quality, coverage, and quantity, as well as having a great variety in values, was chosen in the Fram Strait. It is situated in-between the Arctic Ocean in the north, the Greenland Sea in the southwest, and the Norwegian Sea in the southeast (Fig. 1). The study area encompasses data within the xy-coordinates -509050.000x - 922950.000y in the Upper Left corner, and 397050.000x -1439050.000y in the Lower Right corner, in EPSG:3996 (WGS84 / IBCAO Polar Stereographic) (Spatial Reference, 2008), with the elevation values spanning between 6062 m below mean sea level (MSL) to 1706.91 m above mean sea level. This area encompasses known bathymetric and topographic features, the former of which are of primarily importance in this study. Undersea features within the study area include the Knipovich Ridge, the Molloy Hole, the Lena Trough, the Spitsbergen transform fault, the Molloy transform fault, and the Molloy Ridge along the center of the area (Fig. 3). In addition, iceberg plough marks, continental plateau, continental slope, abyssal plain and seamounts are featured identified in the study area (Fig. 3). The existence of several different seafloor features, which vary in sizes and shapes, is of advantage as they will differ in tendency to be preserved and/or portrayed as the data is processed. By comparing the differences that form due to the different gridding algorithms, the suitability of the methods used for a specific area or type of data can be explored, judging by the artifacts created.

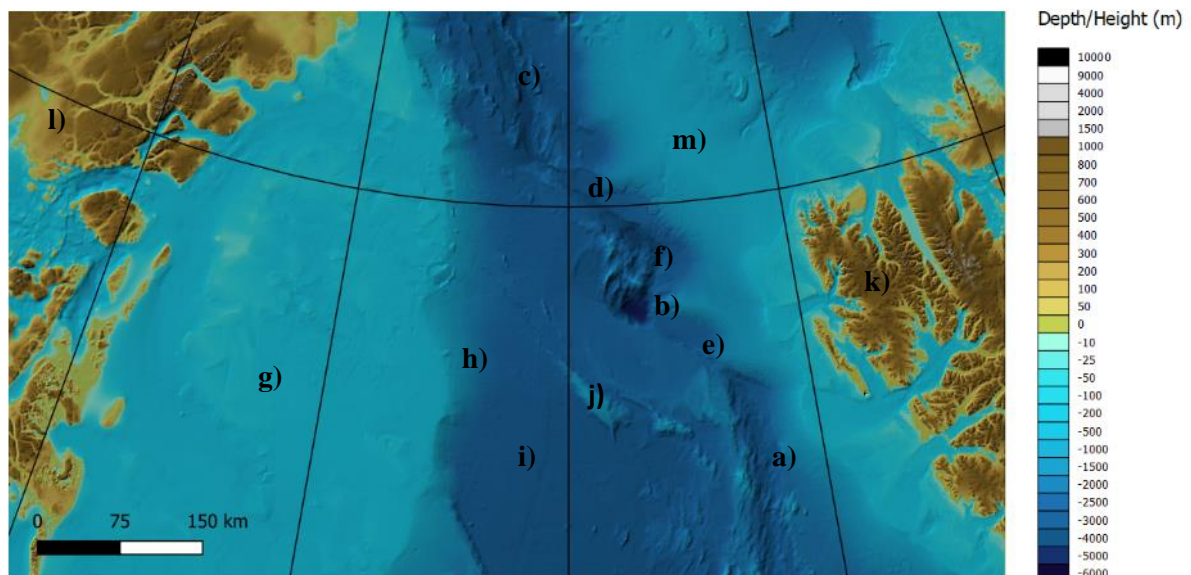


**Figure 3:** The study area triangulated with cell size 100 meters. a) Knipovich Ridge, b) Molloy Hole, c) Lena Trough, d) Spitsbergen transform fault, e) Molloy transform fault, f) Molloy Ridge, g) continental plateau, h) continental slope, i) abyssal plain, j) seamounts, k) Svalbard, l) Greenland, m) Yermak Plateau.

This area has a satisfactory coverage of data, as there are both sections with dense coverage from a multitude of reliable sources, as well as sections of sparse coverage, where interpolation between data points will be of great necessity for creating a DBM. The data are from an updated version of the database used to compile IBCAO Version 3.0 published in 2012 (Jakobsson et al., 2012). IBCAO has become a part of GEBCO (General Bathymetric Chart of the Oceans), a global seafloor mapping project under the International Hydrographic Organization (IHO) and the Intergovernmental Oceanographic Commission (IOC). IBCAO contributes with the Arctic Ocean bathymetry to the World Ocean GEBCO DBM, which was released as a grid of 30 arc-seconds in 2014 (Weatherall et al., 2015). A new update at 15 arc-second has just been released (GEBCO Compilation Group, 2019).

The source data of IBCAO originates from a multitude of sources, and have been collected and combined by IBCAO for the purpose of making a publicly available map of the Arctic Ocean for scientific as well as educational studies and for all other purposes. These data, have been collected using a variety of different methods, such as singlebeam and multibeam swath sonar, both which record the two-way traveltime (TWT), and which then are used to calculate the depth to the seafloor (IHO-IOC-GEBCO, 2014). The TWT is converted to depth in meters by the use of measurements by a CTD (conductivity, temperature, pressure), which determines the velocity for the signal traveling through the water column. The quality of the sound speed control is critical, poor control will lead to different depths in the same area.

As well as there being different methods of gathering the data, there were also different organizations and agencies that conducted these measurements, and provided the collected data to the IBCAO project (*Appendix 2.4 Source files*). Amongst these providers, were Norwegian fishermen through the *Olex* Company, and the U.S Navy through single beam surveys released from submarine surveys (Jakobsson et al., 2012). More traditional sources of bathymetric surveys have been sourced as well, such as GEUS (Geological Survey of Denmark and Greenland) for industry, or MAREANO mapping program for high resolution bathymetric documentation (Jakobsson et al., 2012).

### 3. Material and Method

The different algorithms used in this work to produce DBMs from the source data were applied through the software packages GMT and QGIS 3.4 Madeira's SAGA. The selected algorithms are *surface* done without *blockmedina*, *triangulate*, *surface* done after *blockmedian*, and *Simple Kriging*. The grid files created in GMT 5.3.3 are in NetCDF (.nc) format implying that and they could be displayed in QGIS, where the project map was setup in the coordinate projection as *WGS 84 / IBCAO Polar Stereographic* (ESPG: 3996).

#### 3.1 Python

The original bathymetric source data were provided in one ASCII xyz file. The format was not readily readable in all software. To make the data readable formatting was carried out using Python. This process was done with a Python-code with the function *copyfile*, which was imported from *shutil* (*Appendix 1*). The changes done, was the type of file that contained the data, so instead of .xyz it was in a .txt file. This did not cause any changes to the data within the file, but simply changed the type of file the data was contained within, which ensured that all programs, modules and software could read the file.

#### 3.2 Fledermaus

To reassure that the data had been properly formatted using Python, the resulting output file was displayed in Fledermaus using a Weighted Moving Average (WMA) over a variety of cell sizes. This later lay as foundation for the decision regarding what cell sizes to use when gridding the data in GMT. The cell sizes tested were 75, 100, 175, 200, 250, 300, 500, 1000, and 2000 m. The coordinates system for input and output files were set to *FP\_WGS\_84\_IBCAO\_Polar\_Stereographic*, the one that the original data was assigned in (also identifiable as EPSG:3996). The WMA reduces the influence of the furthest away data, on the resulting data, as a triangle number is used as denominator, which is the sum of each weight/value used (Devic, 2010). Weight Diameter was set to 3, as this would provide a relations in-between data points at a short distance and force the cells to stay close to one another. Data Bounds and DTM Cell Center Properties, which were based of Bounds and Cellsize, amounted to; x-min: -508997.057, x-max: -923000.000, y-max: 395999.998, y-min: -1438999.998, z-min: -6062, and z-max: 1706.91. These were generated by the Fledermaus program identifying the max x, y and z values in the file. Furthermore, to make the contrast between depth and shallow features more distinct, the color map *IBCAO\_ver1.cmap* was used to display the grids.

### 3.3 GMT

The GMT (Generic Mapping Tools) is an assortment of 80 command-line executables with tools appropriate for processing, analyzing and displaying geospatial data, such like the bathymetric data used in this project. Three main executable command-lines used for the three programs run through GMT were *surface*, *gmtselect*, *triangulate*, and *blockmedian*.

Prior to running any of these modules, and after the input (.txt) file had been prepared, each session were initiated by ensuring that GMT could find the .txt file. This was done by running the simple *gmtwhich* module (see *Appendix 2*), with the argument *-C*, which would return a y/n answer regarding whether GMT could locate the file specified. Once the answer returned was y, the modules for interpolation could be run.

#### 3.3.1 Surface Spline with Tension

The module *surface* was used to interpolate a regular grid from the source data points. It creates a smooth surface in-between data points where the smoothness depends on the tension factor and the Laplacian operation (Smith and Wessel., 1990) (Wessel et al., 2017). The equation utilized by the module for interpolation is

$$(1 - T) \times L(L(Z)) + T \times L(Z) = 0 \quad (1)$$

where T is tension factor and Z is the z-value. L is Laplacian operator which is defined by the gradient's divergence in the function. The arguments specified for this operation were *-R* for identifying the coordinates of the AOI, *-I* for defining the cell size for the grid that was to be produced, *-G* for defining the name, destination and type of file that the grid was to be in, *-ll* for defining the minimum acceptable Z-value, and *-Lu* for the maximum acceptable Z-value (*Appendix 2.1.1 -T0*). The specification of max and min in Z-values were a precaution, to prevent the impact of eventual outliers that might have been created by the module (Smith and Wessel., 1990) (Wessel et al., 2017). The values for AOI and Z were derived from the displayed surfaces in Fledermaus, as those values were generated through gridding of the raw source data, which had not been altered by the use of GMT modules for DBM creations. The *surface* module was run in 2 sets, where the first set had the default minimum curvature tension factor of 0 (*Appendix 2.1.1 -T0*), and the second one had the specified maximum curvature tension factor *-T* of 1.0 (*Appendix 2.1.2 -T1.0*). The lower *-T* value would be preferable for rather flatter seafloor, while greater *-T* were preferable for steeper areas. Other than the different *-T*, there were no difference in the arguments specified in the programs, and they were all run to create grids with cell sizes of 100, 200, 250, 500, 1000 and 2000 meters.

#### 3.3.2 Triangulation

The module *triangulate* in GMT was used to produce a Delaunay triangulated surface, and the files created have triplets of id number for each point, which is to identify the position of the point (Wessel et al., 2017) (Watson and Philip., 1983). The creation of these many equilateral triangles, as such geometric forms is what the module strives to create when interpolating the datapoints, will create large files and use significant memory and processing time. This is due to that the Delaunay triangulation uses the method of nearest neighbor to create the equiangular triangles (Watson and Philip., 1983). The original file was first divided into 4 sections that were of similar sizes of between 4,000,000 kB and 3,000,000 kB, with the exception being the subsection with the largest area, which had the smallest file size of just over 400,000 kB. The largest area were the western half (*Appendix 2.2.1 West*), the second largest were the northern part of the east half (*Appendix 2.2.2 North East*), and the southern part of the eastern half was divided into a northern (*Appendix 2.2.3 North of South East*) and a southern half (*Appendix 2.2.4 South of South East*). The eastern half of the AOI contained significantly more data than the western half, as it contained the *SO\_DTM50.xyz* file data covering Svalbard, which was the largest of the source files. This caused the reason as to why the whole dataset had to be subdivided so many times to make it possible to triangulate. The subdivisions were done in GMT with the module *gmtselect*, which required that the original file was specified, as well as what

coordinates from chosen file were to be encompassed in the newly created file. The coordinates for the divides were chosen due to the density of data. The individual areas specified were made to overlap each other slightly to not leave any gaps where no interpolated triangles were created. As for the *triangulate* module, the used arguments were *-R* for the AOI (which this time was specified to be the whole AOI, as opposed to the smaller sections specified for the cut-outs), *-I* for defining the cell size for each individual grid created, and *-G* for directing where and what the new file should be. The sections, once entered into QGIS, were then merged into a single file in batches with the other files gridded with the same cell size, to create the whole surface of the AOI, using *Raster>Miscellaneous>Merge* (Ryan., 2018).

### 3.3.3 Block median

The module *blockmedian* was used as a filtering method, to lessen the concentration of data in accordance with the intended gridded cell size. It is a precaution recommended to be applied prior to the use of *surface*, as it negates the creation of aliasing shorter wavelengths (Wessel et al., 2017). In *blockmedian*, *-I* was used to define the size of the cells, and the value of each of these cells was defined as the median value of all data points encompassed by that specific cell's area (see *Appendix 2.3 Block median*). This was followed by the *surface* module (see *Appendix 2.3 Block median*), which interpolated the cells defined in *blockmedian*, to create a surface in the expanses in-between the data. The AOI was specified with *-R*, the file to be created was given by *-G*, and the maximum respective minimum Z-values were defined with *-Ll* respective *-Lu*.

## 3.4 SAGA Kriging

The fourth method of interpolating data and creating surfaces from the Fram dataset was through simple kriging, which was done using SAGA (System of Automated Geoscientific Analyses) in QGIS. This program, since it was an integrated part in the QGIS module, needed to have the Fram Strait data accessible within the project before it could be processed. The data was imported as a delimited text file, projecting in QGIS as every data point being an independent vector point unconnected to the others. As the full file was significantly larger than any of the previously created files, it could not be utilized in its entirety, and instead only the first 1,048,576 rows of the data were used, entered via smaller files containing 110,000 rows each.

### 3.4.1 Simple Kriging

The kriging method used were the one designated as “Simple Kriging”, which ran on a basic formula of

$$a + b \times x \tag{2}$$

(Conrad., 2015). Simple Kriging creates an interpolation by describing the covariance of a variable to another, and thereby giving the spatial covariance of the field. The parameters that were utilized for the kriging were set to default (Conrad., 2015), with the exception for attribute, which was set to the Z-values, the type of Quality measure, which was defined as [1] variance. As well, the cell size and block size were set to be of the chosen size for that particular grid that was being created. Once all the parts were run through the function, they were merged into a singular file in the same manner as the triangulated files were.

## 4. Results

### 4.1 Fledermaus

The surfaces created from the raw data in Fledermaus, were due to their variety in cell size, capable of showing different degrees of details. This was due to the finer grids including more of the data, as the original data was less blanketed by large cells. The larger cells covered up more data points, which would smooth out the surface.

The surface with 75 m cell size proved to have many problems, as it created artifacts in areas where the data coverage was too sparse. These would generally be in deeper areas, such as on the deep ocean plain, or on the Molloy Ridge and in the Molloy hole. As for the higher resolution shallow depth data, which were provided mostly by Olex and various multibeam cruises, had a better coverage, and was favorable for showing smaller features. The areas that are covered by the higher resolution grids, are in shallower waters, that are well-traversed by continuous vessel traffic, such as by fishing vessels (Jakobsson et al., 2012).

In Fledermaus, an assortment of different features can be observed, as well as artifacts of varying degrees. The finer grid, as in the grids with the smallest cell sizes, has a larger assortment of visible artifacts, as well as features, which are not observable with the larger cell sizes. Such features were iceberg plough marks, which can be seen along the coast of Svalbard and on the shallower sections of the Yermak Plateau, where they are visible up until a cell size of 500 m, where they then became too alike the track of the multibeam line to be properly identified. The iceberg plough marks could be seen in QGIS in the smaller cell sizes, in the same region.

On the other side of the spectrum, the artifacts revealed in Fledermaus were many, and differed in appearance and areas of occurrence. One artifact, which were predominantly created by the multibeam in the deeper sections of the AOI, were a tartan-like pattern of squares, which had depressed values compared to their nearest neighboring data points, which then stood up like stalagmites (Fig. 5). This type of artifact was most prominent below the cell size 250 m, indicating that the cell size was too small or the data coverage. They were not seen in coarser grids. On more shallow areas, such as the Greenland Plateau, small elevated single dots could be seen where single-point measurements had been taken by a ship passing through (Fig. 4). Similar in nature were esker-like artifacts that could be seen winding across the shallow sea floor, as well as deep gouges in fjords (Fig. 4). These were all created due to the difference in elevation of these data points, in comparison to the surrounding data, and much like other artifacts and smaller features, they could only be seen in the surfaces created with smaller cell sizes.

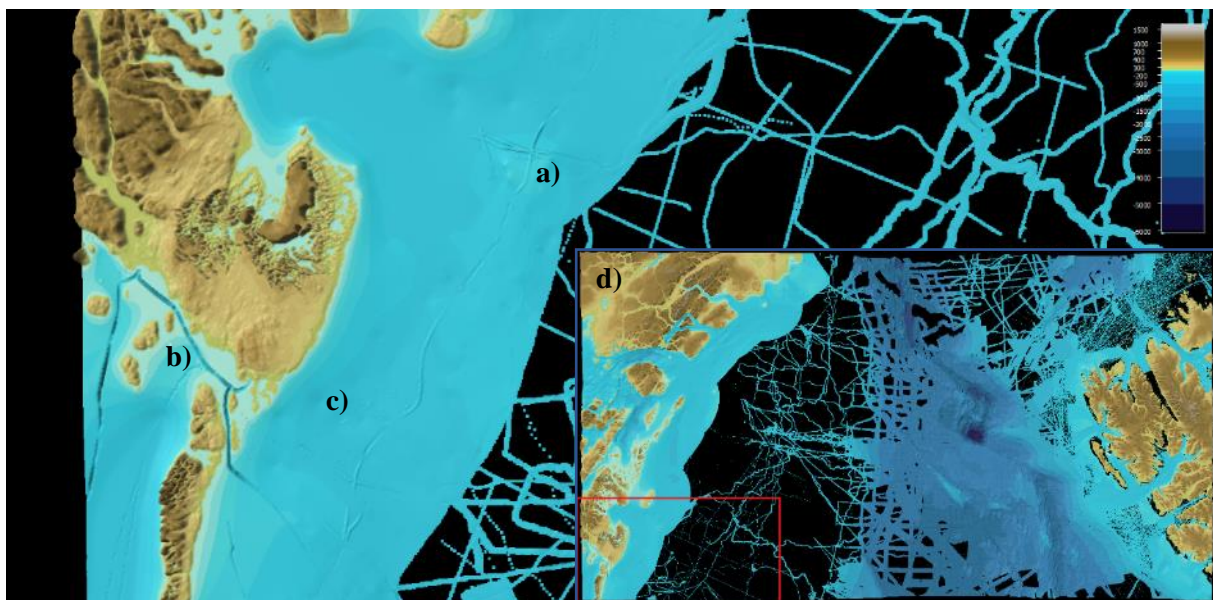


**Figure 4:** Artifacts a) “eskers”, b) “trough” and c) “dots” shown in Fledermaus. Cell size 250 m. d) shows the area within the study area, marked with a red square.

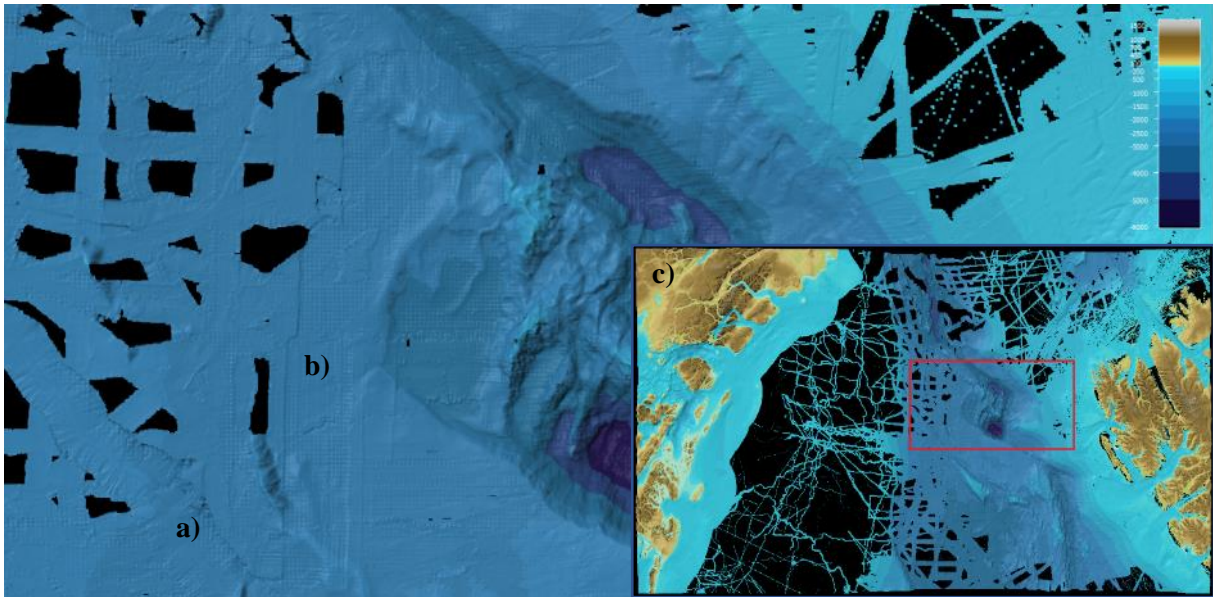


**Figure 5:** Artifacts a) “tracks” and b) “tartan” shown in Fledermaus. cell Size 200 m. c) shows the area within the study area, marked with a red square.

## 4.2 GMT

### 4.2.1 Surface Spline with Tension

The *surface* module, as stated in 3.3.1 *Surface Spline with Tension*, was run with two different extremes of tension factors; the default of 0, and the specified one of 1 (Wessel et al., 2017) (Smith and Wessel., 1990). The tension of 0 resulted in a smooth surface, which had the ability to curve unhindered and create local minimum and maxima independent of the established data values. The tension of 1 created a strictly defined surface in-between the data points, with no spline possible. These single differences presented themselves in the location of formed artifacts in the grids with finer cell sizes. For both  $-T$ , aliasing occurred of data originating from specific lines, which resulted in a pattern of the possible maximum and minimum Z-values to appear as a diagonal pattern resembling of a zebra crossing (see Fig 5.) (Wessel et al., 2017). These artifacts formed on the abyssal plain, as well as some on the Greenland Continental Shelf, the Yermak Plateau and the continental slope, and only in sections where there were good data coverage. These zebra areas only showed on grid sizes 100 and 200 m for  $-T0$ , while  $-T1.0$  had aliasing showing in 100, 200 and 250 m. The areas affected with these, though, were not the same, as the artifacts were far smaller, and did not encompass large stretches of data. The  $-T1.0$  grid with 250 m resolution were the one with most notable aliasing, as they were vertical, and only occurred in the center of the AOI, significantly over the Lena Trough.

Another identifiable artifact in these files were false depressions and hills/seamounts (Fig. 6). The depressions were caused by undershoots, while the elevations were due to overshoot as a response to the filtering process, where there is a leap in values done due to the low tension in  $-T0$ . For  $-T1.0$  they could only be seen vaguely on the Greenland Continental Shelf as large areas with discreet but homogenous depression, while  $-T0$  were heavily disturbed by them along the Greenland Continental Shelf in-between single beam data provided by industry from seismic profiles (Jakobsson et al., 2012). Sharp elevations had also been created on the abyssal plain, the continental slope, and the Lena Trough. The depressions were clearly formed where there was interpolation done, as the surrounding data align with the positioning of data in Fledermaus. These depressions and elevations could only be found, for both  $-T0$  and  $-T1.0$ , on the grid with cell size 200 meters.

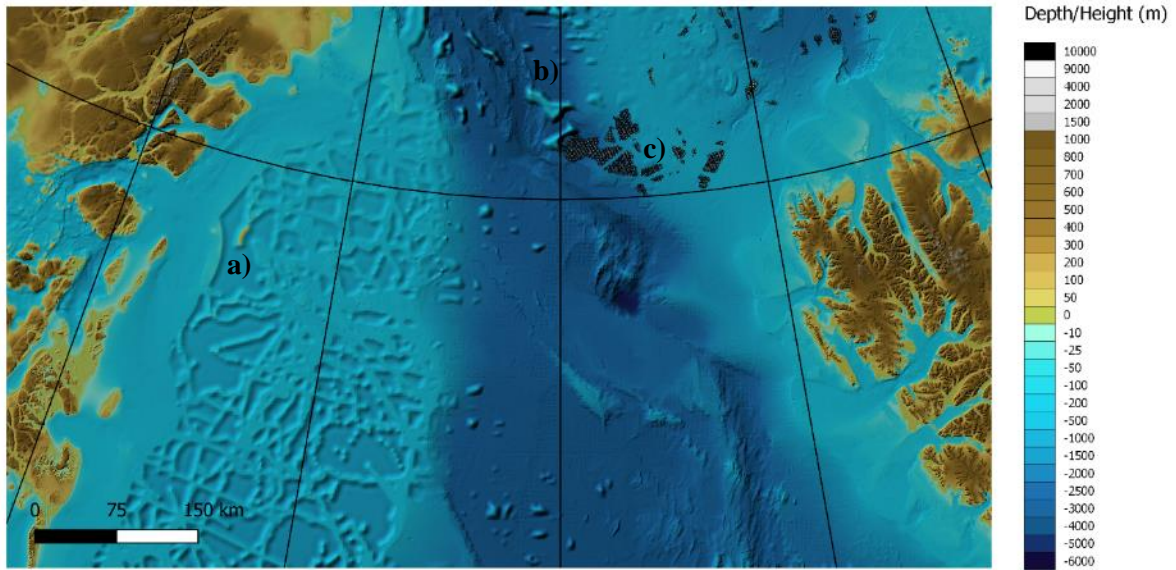


**Figure 6:** AOI with artifacts a) “depressions”, b) “elevations” and c) “zebras”, gridded with *surface - T0*, cell size 200 meters.

#### 4.2.2 Triangulation

The *triangulate* module, as stated in 3.3.2 *Triangulation*, was used to create four separate DBMs, which then were merged to encompass the entire AOI. The artifacts that appeared when applying *surface* did not show up in the triangulated DBM. Instead there were a risk of there being straight mono-valued lines created along the edges of the areas that did not properly overlap each other, and therefore creating a long elevated (or in some parts, depressed, depending on the surrounding data) line across the AOI. This was avoided by having the subsections overlapping each other, so there would be no space within the AOI that did not get triangulated. The triangulation did not create any noticeable artifacts, and as this was the case, all different cell sized grids were preserving features without them being disturbed (Fig. 7). The single type of artifact formed thru TIN were facets, which were large triangles that spanned in the space in-between data points (Fig. 7). The facets were noticeable, as they were significantly larger than the surrounding triangles, and therefore created a large area with little variation in the surface.

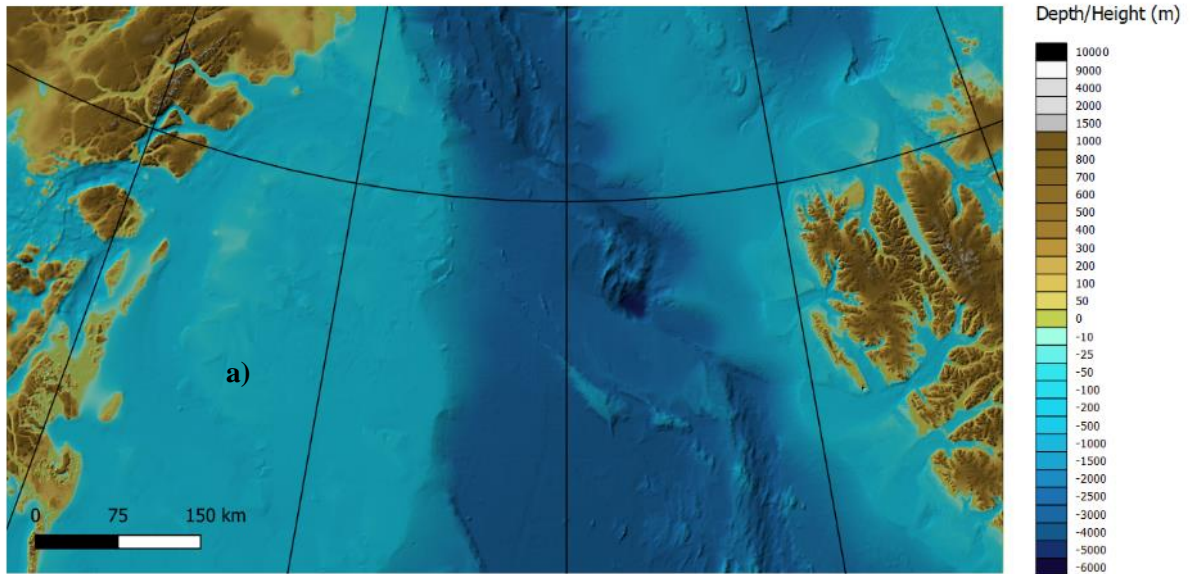


**Figure 7:** AOI gridded with *triangulate* and merged, showing a) showing “facet” artifact. Cell size 100 m.

#### 4.2.3 Block median

As was stated in 3.3.3 *Block median*, the *blockmedian*, followed by a simple *surface* gridding created .nc files that had reduced content of data, as they had been filtered to sport only the data necessary for gridding of the specified cell sizes. The artifacts created in these were of the same aliasing nature as in the 3.3.1 *Surface Spline with Tension*, though they were much smaller, and only occurred on the Yermak Plateau in the grids with cell sizes of 100 and 200 meters. These artifacts seemed to be caused when gridding of files such as the multibeam *ark20\_3\_IBCAO\_PS\_100m\_edited.xyz*. Apart from this, the AOI gridded with no visible disturbance (Fig. 8).

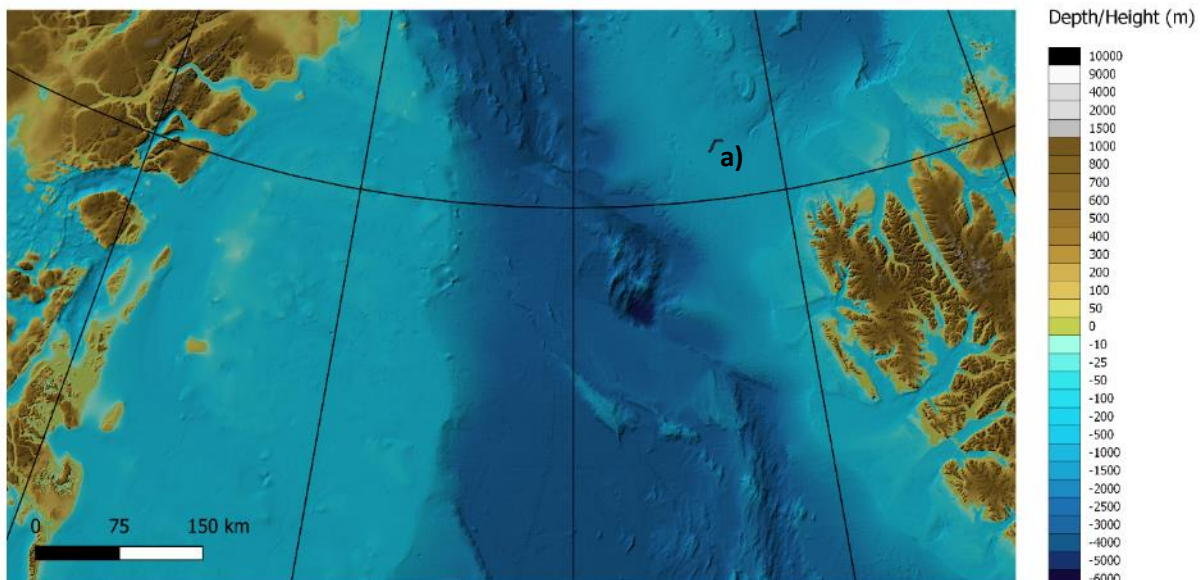


**Figure 8:** AOI gridded with *blockmedian* and *surface*, showing artifact a) “zebra”. Cell size 100 m.

## 4.3 SAGA Kriging

### 4.3.1 Simple Kriging

The *Simple Kriging* algorithm available in SAGA through QGIS was only capable of handling a smaller part of the data in the AOI, as stated in 3.4.1 *Simple Kriging*. A grid was produced for the Molloy Ridge, Molloy Hole, and Lena Trough area. For this reason, only artifacts in this deeper part of the AOI could be compared with the other methods. The artifact that was observed, was seen as the tracks laying on-top of one another where they crossed one another, and the most elevated data being on-top of the lower grids (Fig. 9). The elevation of the different tracks, was caused by the difference in Z-value, caused by different sound velocity profiles for the different voyages.

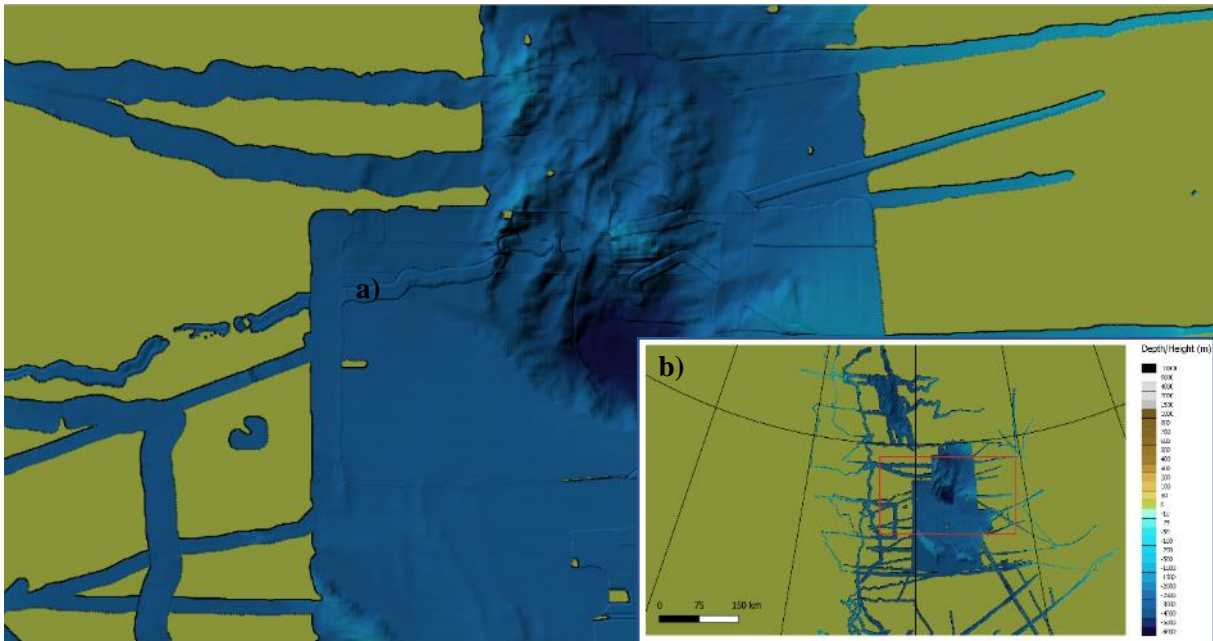


**Figure 9:** Partial gridding of AOI, done in *Simple Kriging*, showing artifacts a) “tracks on top” (in Molloy Hole). Cell size 100 m. b) shows the area within the study area, marked with a red square.

## 5. Discussion

The different bathymetric data sources, as stated in 2.1 *Geological Setting*, and the different methods of gathering data, imply a number of possible errors and artifacts. For example, in response to factors such as the state of the equipment, the conditions of the weather at the time of the recording, as well as possible human errors (IHO-IOC-GEBCO, 2014). Artifacts could have occurred from oceanographic changes in the water column, which would affect the traveltime of sound pulses, and with an outdated CTD (conductivity-temperature-depth package) or XBT (expendable bathythermograph), the depth will then become incorrect (IHO-IOC-GEBCO, 2014). In deeper areas, refraction for the outer signals could also become a problem, which creates false depth for the returning signals, as refraction created due to differences and shifts of the CTD-created sound velocity profile in the water column would alter the angle and travel distance for the signal, resulting in artifacts being created (IHO-IOC-GEBCO, 2014). Older data necessary for creating DBMs was at times gathered by smaller vessels, or vessels with less than optimal positioning, even prior to the time of GPS. The coordinates registered for the data might therefore be off, which would result in data that might be correct in value, but displaced (IHO-IOC-GEBCO, 2014).

### 5.1 Fledermaus

As the sizes of the cells gridded in Fledermaus varied, so did the quantity of data points being saved and displayed on the created surface. The larger cells would cover large amounts of data compared to the smaller cell sizes. This resulted in the loss of data with the larger cells, but a possibility of a

smoother transition between projected data points. The larger cells would also result in the maximum and minimum values being lessened in their extremes, as the value of the individual data point were lessened with the greater cells, as they would include more data to form each cell, and the data points would weight upon each other to give a middle value that the cell would represent. As for the smaller cell sizes, the outliers and false values were given more weight, as there were a reduced number of more probable values to correct the value assigned to the cell, which is what negated the extreme values when larger cells were applied. This may very well be the reason as to why such artifacts as the tartan pattern occurred, as the multibeam-created artifacts would be given more weight upon the grid, as they were not negated by the surrounding data. Areas greatly affected by these tartan patterns, were the deeper sections, such as on the ocean plain, or in the Molloy Ridge and Molloy hole. This would be due to the data of the deeper sections of the area had been gathered less frequently, due to the greater depth allowing for the signals to spread more before hitting a surface and return (Jakobsson et al., 2012). At the deeper sections of the study area, the distribution of data points would therefore be greater, which in turn would make the use of smaller cell sizes unfavorable, as they were not able to properly cover the empty space in-between.

Due to the density of the artifacts observed in Fledermaus, as well as what features could be seen at the different cell sizes, the sizes for the .nc files were decided to be 100, 200, 250, 500, 1000 and 2000 m. 100 were the smallest that could be comfortably run, while 250 being the best choice for keeping features at the same time as artifacts were lesser (Fig. 10). 2000 was the largest that one could do and keep the general look of the major features on land (which were the area with the densest data coverage). These observations are the result of the difference in-between the horizontal resolution of the area, as it interacts with the chosen cell sizes. The horizontal resolution is dependent on the quantity of the data, the beam footprint, and the bottom detection mode (Jakobsson et al., 2016). Too few data points in a cell would pronounce artifacts, as they are given more weight than they should in the final grid due to there being too few correct data points to outweigh the artifacts. Too much data covered in a single cell will risk the loss off features, as the data points are weighted down by other data points. In accordance with the equation for defining the footprint diameter  $Df$

$$Df = 2H \times \tan\left(\frac{\alpha}{2}\right) \quad (3)$$

where  $H$  is the depth of the surface from the transducer, and  $\alpha$  is the opening angle that the multibeam exits through, the size of the signal when it hits the sea floor can be calculated (Jakobsson et al., 2016). For a  $2^\circ$  angle at a depth of -3500 meter (a common depth on the abyssal plain in the AOI), the footprint diameter would be 122 meter, double of which is close to 250 meter, which is the best cell size for preservation of features, as well as avoiding artifacts.

The artifacts seen in Figure 4 have been created due to the difference in Z-values for the different datasets used in this same area. This would be an indication of the TWT derived from the CTD velocity being different in the different expeditions. This is the same origin, or the tracks seen in Figure 5, which too are formed due to differences in the estimated sound velocity profiles. As for the tartan pattern seen in Figure 5, they are an artifact created due to the chosen cell size being unfavorable with the scarcity of data points, which explains why they disappear when larger, more blanketing, cell sizes are adopted.

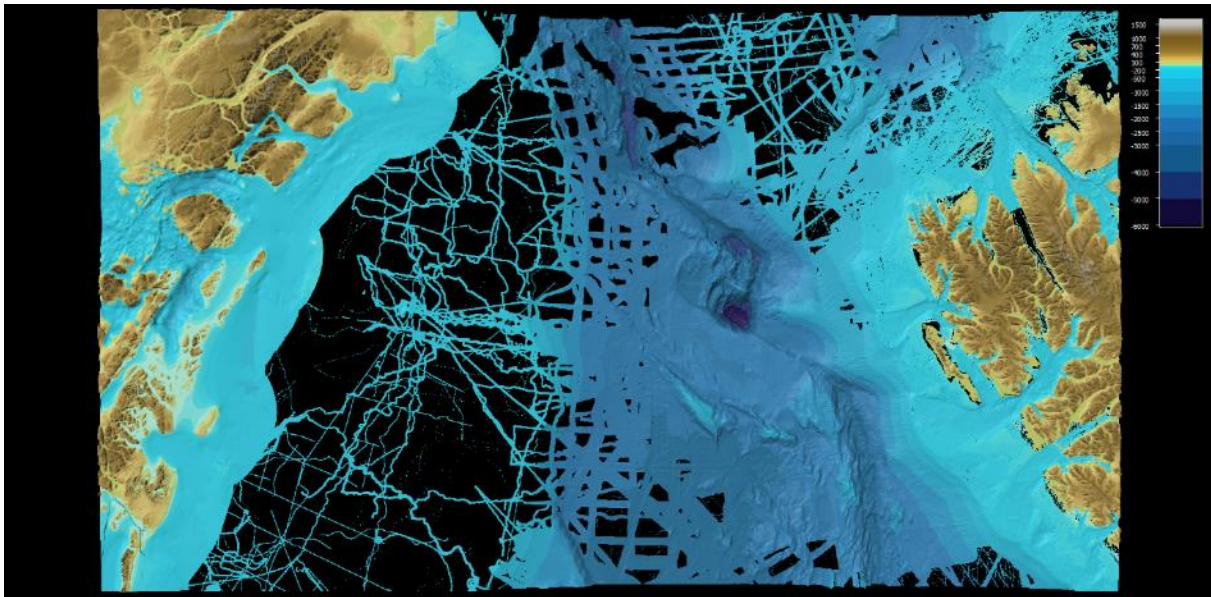


**Figure 10:** AOI displayed in Fledermaus. Cell size 250 m.

## 5.2 GMT

### 5.2.1 Surface Spline with Tension

The *surface* module, with its interpolation by tension factor and Laplacian operation-dependent function, created varying degrees of acceptable grids, as there were varying degrees of artifacts created that covered the AOI. The finer grids, though preserving more of the finer details, features and shapes that the dataset included, had a tendency to preserve and accentuate any artifacts created (Hell and Jakobsson., 2011). This was not a particular problem observed in the grids with larger cell sizes, as artifacts did not occur when the gridded cells were above 250 m, in the same manner that finer features were not preserved either. This loss of details, both wanted and unsought, was a phenomenon caused by the filtering of data that was conducted by the *surface* module that GMT was gridding the data in accordance with the parameters dictated by the code. Not only did the module need to create interpolations, but also, it needed to choose what value to assign the created cells in the grid, something which was done based on what data was present at the specific area that would entail the specified cell, or by interpolating based on the nearest available data points.

The most striking artifacts created, were the zebra crossing-like aliasing shapes, which occurred in areas with good data coverage (Hell and Jakobsson., 2011). These artifacts, which showcased values of maximum Z and minimum Z neighboring each other, were easy to distinguish as false features, as no such features made an appearance in the grids with larger cell sizes, nor did they occur in the Fledermaus surfaces. This would therefore indicate that they were not natural features, and that their origin was an error, based on how the GMT module chose data from the source, and then proceeded to project it in the created surface. It could be speculated that, due to the overwhelming data available at those specific locations, especially as different data bands from different voyages could provide differing data for the same area, the module would become biased to specific values in one cell, while showing favor for another data value in the neighboring cell, as the data provided within it would be differing. This would not be a problem with the larger cell sizes, as they would be canvassing enough area to include a variety of differing data values, and would thereby create a cell with a value that was weighted down by a great number of different Z-values, and the majority would be in the correct aspect of the elevation scale. Furthermore, the aliasing was caused by the module, as the overwhelming amount of data accessible for the *surface* module would create spatial aliasing for shorter wave-lengths. This would be an acceptable explanation, as these types of artifact did not occur in areas where data coverage was poor or non-existent, as these zones would have greater wave-lengths. Interestingly, the difference in tension factor resulted in a difference in where the aliasing

shapes could be located. With  $-T$  set to 0, and therefore creating a smoother surface due to the minimum curvature, which in turn runs the risk of creating false minimum and maximum Z-values in local settings, such as these artifacts observed here. In contrast,  $-T$  defined as 1 would have given the maximum possible curvature, which would be preferable in steeper areas, as the data will be interpolated harmonically, and no local minimum or maximum should be created other than at controlled data points. As there still could be observed artifacts of this striped nature, even though the  $-T$  was defined to hide the occurrence of such, would indicate that it was the overwhelming amount of available data that caused the module to create these false features. It is of interest to note that the  $-T$  value that were to prefer for flatter surfaces, created artifacts in the very areas where the data were most homogenous, while the  $-T$  best suited for steep areas created artifacts in the steepest areas in the AOI.

The second artifact observed in the displayed *surface* grids, were the false elevations and depressions. These would form in-between known data in the shape of steep depressions, or above deeper data as seamount-like shapes. They had in common their steep sides from the known data, to the surface of interpolation, which was generally flat. These false features only occurred in the in the grid with  $-T0$  and cell size 200 m, while similar minor depressions and elevations could be hinted in the  $-T1.0$  with the same cell size and same area, the Greenland Continental Shelf. This might indicate that this method, in combination with the particular density of the data in that area, were not of favorable nature to one another, and therefore would easily create these artifacts when these specific factors were as such.

Even though the data surrounding the artifacts seemed to resemble the Fledermaus project faithfully, the great total area covered by the artifacts resulted in much of the AOI not being usable for a faithful projection of the sea floor, and thusly this method of operation would not be recommended for similar projections of data of comparable nature as the one used in this study, if one were to do a projection that were to preserve and showcase smaller features. If the goal was to create a projection with the acceptable cell size being 500 meters or above, then this method could be utilized.

### 5.2.2 Triangulation

The *triangulate* module created one particular type of artifact, it being large triangular and flat facets, which stretched out in and filled the larger gaps of data in the AOI. These artifacts stood out greatly from the rest of the TIN, as there were no shifts in the surface due to the created triangles, assuring that the contrast would not be missed. Though, as unnatural as they appeared, they did not deter from the well-gridded sections of the AOI, as the values of the facets were not alien in their areas.

In the areas defined by good data coverage, the features were properly preserved even in the finest grids used. This would be as the triangulating module is not prone to create local extremes in minimum and maximum in the interpolation, as the wavelengths will be focused on being as equilateral as possible, and therefore only create data that is in-between the known data points that the interpolation is supposed to fill in. No matter if the data coverage was poor or rich, or if the surface was steep or flat, the triangulation created good grids in all the tested cell sizes, and the features that were to be expected were preserved. This method would have been good for a smaller data set, no matter the nature of the surface it was representing. But for a larger data set, like the one used in this project, the module would have required too much data to be able to create one single file for the whole AOI, and therefore there was a need to subsection the AOI to data files that were manageable for the module. This would result in the data points that were by the border of the individual subsection had no data points to interpolate with. As such, if the individual sections were to be merged into a single file after they had all been gridded, there would be a gap in the joints where no data had been gridded, which would have resulted in a mono-valued line stretching across the area. This potential artifact was negated by having the different subsections overlapping each other slightly, which would result in there being data everywhere when the sections were later merged into one raster.

As this method, though slightly convoluted due to there being a need of manually defining the coverage of each subsection, did produce the most reliable and probable grid, as there were no artifacts to be found, and thereby the results were trustworthy as a probable projection of the sea floor. This method, despite being the one requiring the most of the operative conducting the project, did present the best results, and therefore it is thought that this module is to be strived for usage, if the time for data handling allows for it. The non-existence of artifacts, as well as the great preserving of features and data defines this method of modeling to be the best for this type of dataset, where there is a great difference in data coverage, as well as types of surfaces to be connected and created.

### 5.2.3 Block median

The zebra-reminding aliasing areas were significantly smaller in the *surface* grids, when the file had not been run thru with *blockmedian* beforehand. This, most certainly, is due to the great downgrade of data available in the file used for the gridding, in comparison to when the data was run thru the *surface* module unprocessed. This meant that, once the *surface* module was to access the data available and convert them to an interpolated grid, there had already been a sorting and cleansing done, making it so that the data that were accessible for the module were previously defined, and chosen from the data in the original file, without the need of creating any interpolations or specific correlations in-between the datapoints. The chosen datapoints in the Block median file were defined singularly by what values could be found in that particular area for that specific cell, and mostly, despite there being just as many questionable data values available in the original file, the resulting cells still favored the Z-values that would naturally be more homogenic with the surrounding values. Spatial aliasing would be less of an occurrence naturally, as the distance in-between data points would be greater, and the fewer short wave-lengths that would have to be created thru the interpolation via *surface*, the lesser the risk of there being created extreme local minimum and maximum Z-values.

As this gridding had little interference of artifacts, then even the finer grids could clearly present the finest features clearly, as they were not overshadowed by false features. This would mean that there were much data that were created thru the interpolation which were believable, and which would have a great probability of being true to reality. As the known data points were defined and assumed to be trustworthy, then the interpolations in-between were quite possibly trustworthy for projecting and presenting a trustworthy representation of the sea floor in the AOI.

The created grid thru the use of *blockmedian* before the *surface* created a grid with mostly undisturbed data points, where the projected grid was utterly plausible, as the artifacts were few and small, and as they were created in areas where there would have been many short wavelengths of the data had not been purged beforehand, then a defining *-T* of approximately  $\sim 0.25$  would suffice in negating the most extravagant minimum and maximum created. As such, it could be deduced that for the AOI that has been used in this project, this method is quite favorable for gridding data in a plausible and realistic manner, for large cell sizes as well as for finer cell sizes.

## 5.3 SAGA Kriging

### 5.3.1 Simple Kriging

Due to the restrictions put up by this method, the data could not be satisfyingly processed and gridded for a proper evaluation and comparison with the other methods to be conducted. What little area that could be produced and processed with this module were, and it created recognizable artifacts that appear on the finer cell sizes of the grids created thru the GMT modules.

The crossing of the gridded lines creating what could be mistaken for iceberg plough marks, though their location at a depth of  $< -5000$  mbs makes such origins unlikely. These artifacts were formed as the *Merge* in QGIS favored the most elevated data over when merging the grids into one raster file, as this would be how they were to appear if all the surfaces were projected on top of one another. The difference in z-value in-between the smaller individual grids is a testimony to how the datapoints carry different values due to the being from different voyages, with different sound velocity profiles. When

they are processed without relations to the data that should be in direct association with them, as opposed to how they appeared in most of the other methods used, the neighboring data points have no direct influence in the resulting Z-value appointed to a datapoint after processing, as they were not available to one another during the processing. It is also notable that in the area where no data has been plotted, *Simple Kriging* assigned the value 0 to all fields, causing the great green sea around the data that was plotted (Fig. 9).

This method could, due to the less than optimal results as the execution of the operation was hampered by the nature of the dataset itself, be decided to be the least preferable of the tested methods during this project, as the dataset was too large for this type of module to be used properly and efficiently.

## 6. Conclusion

This project utilized four different methods for interpolating data and creating a grid, in the purpose of observing in what different ways the data would be presented in. The data was plotted in Fledermaus for reference, as this program did not produce any interpolation, though it did smooth the values through Weighted Moving Average. The first method of interpolation, *surface*, was done with the tension factor 1 and 0, where it was observed that with established  $-T$  at 1, there were less aliased data created, as well as other false features. The second method, *triangulate*, was the most successful in creating a good end result of the AOI, which was to be free of artifacts in all cell sizes, and that preserved the features well when the subsections run through this module were overlapping each other. The third method, *blockmedian*, was used to filter the quantity of data, so that when *surface* was run through the now cleansed data. There would be less short wavelengths in-between data, which lessened the possibility of aliased data being created. The last module was the *Simple Kriging* done in SAGA in QGIS. This module could not properly handle large files, and the size of files compatible with this module would require the original file being split up too many times for it to be a good method of choice for this file. So, for the Fram strait, with its great variation of data coverage, quality and quantity, the most successful method of interpolation was by triangulation, as the resulting grid presented with an artifact-free and feature-rich gridding of the data, which could be used successfully for presenting a DBM for the area, based on the data provided. Due to the nature of the dataset used, and the end results, this method would be a good choice in other areas where the data is of similar capability as the data used here.

## Acknowledgment

I wish to thank my supervisor for this project, M. Jakobsson, for his aid, support and suggestions in ensuring that the operating modules used for this project were operational, and as well for presenting me with the opportunity to do this project. Also, I would like to thank R. Mohammad, for providing suggestions for what may be wrong with the program, and for helping in deciphering the Error codes that occurred during this project, and as well, for providing the data set from IBCAO which was used in this project.

## References

- Conrad, O.: *Module Simple Kriging*, SAGA-GIS Module Library Documentation (v2.3.0), 2015.
- Devic, J.: *Weighted Moving Averages: The Basics*, Investopedia, 2010.
- GEBCO Compilation Group: GEBCO 2019 Grid (doi:10.5285/836f016a-33be-6ddc-e053-6c86abc0788e)
- Hell, B. & Jakobsson, M.: *Gridding heterogenous bathymetric data sets with stacked continuous curvature splines in tension*, Marine Geophysical Research (2011) 32: 493. 10.1007/s11001-011-9141-1.
- International Hydrographic Organization, Intergovernmental Oceanographic Commission, The IHO-IOC GEBCO Cook Book, IHO Publication B-11, Monaco, Sept. 2014, 461pp - IOC Manuals and Guides 63, France, Sept. 2014, 461pp.
- Jakobsson, M., Gyllencreutz, R., Mayer, L. A., Dowdeswell, J. A., Canals, M., Todd, B. J., Dowdeswell, E. K., Hogan, K. A., and Larter, R. D.: *Mapping submarine glacial landforms using acoustic methods*, Geological Society, London, Memoirs, 46, 17-40, <https://doi.org/10.1144/m46.182>, 2016.
- Jakobsson, M., Mayer, L., Coakley, B., Dowdeswell, J. A., Forbes, S., Fridman, B., Hodnesdal, H., Noormets, R., Pedersen, R., Rebesco, M., Schenke, H. W., Zarayskaya, Y., Accettella, D., Armstrong, A., Anderson, R. M., Bienhoff, P., Camerlenghi, A., Church, I., Edwards, M., Gardner, J. V., Hall, J. K., Hell, B., Hestvik, O., Kristoffersen, Y., Marcussen, C., Mohammad, R., Mosher, D., Nghiem, S. V., Pedrosa, M. T., Travaglini, P. G., and Weatherall, P.: *The International Bathymetric Chart of the Arctic Ocean (IBCAO) Version 3.0*, Geophysical Research Letters, 39, L12609, 10.1029/2012gl052219, 2012.
- Ryan.: *QGIS: Raster Merging*, Drones Made Easy, GIS Post Processing, 2018.
- Smith, W. H. F., and Wessel, P.: *Gridding with continuous curvature splines in tension*, Geophysics, 55, 293-305, 1990.
- Spatial Reference.: *ESPG:3996*, WGS 84 / IBCAO, Polar Stereographic, 2008.
- Watson, D. F., Philip, G. M.: *Systematic Triangulations*, Department of Geology and Geophysics, University of Sidney, Sidney, N.S.W., 2006, Australia, 10.1016/0734-189X(84)90184-1, 1983.
- Weatherall, P., Marks, K. M., Jakobsson, M., Schmitt, T., Tani, S., Arndt, J. E., Rovere, M., Chayes, D., Ferrini, V., and Wigley, R.: *A new digital bathymetric model of the world's oceans*, Earth and Space Science, 2, 331-345, 10.1002/2015EA000107, 2015.
- Wessel, P., and Smith, W. H. F.: *Free software helps map and display data*, EOS Transactions, American Geophysical Union, 72, 441, 445-446, 1991.
- Wessel, P., Smith, W. H. F., Scharroo, R., Luis, J., Wobbe F.: *blockmedian*. GMT 5.3.2 documentation, 2017.
- Wessel, P., Smith, W. H. F., Scharroo, R., Luis, J., Wobbe F.: *gmtselect*. GMT 5.3.2 documentation, 2017.
- Wessel, P., Smith, W. H. F., Scharroo, R., Luis, J., Wobbe F.: *surface*. GMT 5.3.2 documentation, 2017.
- Wessel, P., Smith, W. H. F., Scharroo, R., Luis, J., Wobbe F.: *triangulate*. GMT 5.3.2 documentation, 2017.

## Appendix

### 1. Python

```
>from shutil import copyfile
```

```
>copyfile('fram.xyz', 'fram.txt')
```

### 2. GMT

```
>gmtwhich D:/LindaKarlsson-X-jobb/Data/fram.txt -C
```

#### 2.1 Surface

##### 2.1.1 -T0

```
>gmt surface D:\LindaKarlsson-X-jobb\Data\fram.txt -R-509000.0/396200.0/-1439000.0/-923000.0 -I[nr] -Gfram_ll[nr]grd.nc -Ll-5568.39 -Lu1607.49
```

##### 2.1.2 -T1.0

```
>gmt surface D:\LindaKarlsson-X-jobb\Data\fram.txt -R-509000.0/396200.0/-1439000.0/-923000.0 -I[nr] -Gfram_llIT[nr]grd.nc -Ll-5568.39 -Lu1607.49 -T1.0
```

#### 2.2 Triangulate

##### 2.2.1 West

```
>gmtselect D:/LindaKarlsson-X-jobb/Data/fram_west.txt -R-509000.0/-5000.0/-1439000.0/-923000.0  
> D:/LindaKarlsson-X-jobb/Data/fram_west3.txt
```

```
>gmt triangulate D:/LindaKarlsson-X-jobb/Data/fram_west3.txt -R-509000.0/397000.0/-1439000.0/-923000.0 -I[nr] -GD:/LindaKarlsson-X-jobb/Data/fram_[nr]_tri_hw2.nc
```

##### 2.2.2 North East

```
>gmtselect D:/LindaKarlsson-X-jobb/Data/fram_east.txt -R-16000.0/397000.0/-1181000.0/-923000.0  
> D:/LindaKarlsson-X-jobb/Data/fram_east2n.txt
```

```
>gmt triangulate D:/LindaKarlsson-X-jobb/Data/fram_east2n.txt -R-509000.0/397000.0/-1439000.0/-923000.0 -I[nr] -GD:/LindaKarlsson-X-jobb/Data/fram_[nr]_tri_he1n.nc
```

##### 2.2.3 North of South East

```
>gmtselect D:/LindaKarlsson-X-jobb/Data/fram_east.txt -R-16000.0/397000.0/-1439000.0/-1181000.0  
> D:/LindaKarlsson-X-jobb/Data/fram_east2s.txt
```

```
>gmtselect D:/LindaKarlsson-X-jobb/Data/fram_east.txt -R-16000.0/397000.0/-1310000.0/-1180000.0  
> D:/LindaKarlsson-X-jobb/Data/fram_east2sn.txt
```

```
>gmt triangulate D:/LindaKarlsson-X-jobb/Data/fram_east2sn.txt -R-509000.0/397000.0/-1439000.0/-923000.0 -I[nr] -GD:/LindaKarlsson-X-jobb/Data/fram_[nr]_tri_he1sn.nc
```

##### 2.2.4 South of South East

```
>gmtselect D:/LindaKarlsson-X-jobb/Data/fram_east.txt -R-16000.0/397000.0/-1439000.0/-1181000.0  
> D:/LindaKarlsson-X-jobb/Data/fram_east2s.txt
```

```
>gmtselect D:/LindaKarlsson-X-jobb/Data/fram_east.txt -R-16000.0/397000.0/-1439000.0/-1300000.0  
> D:/LindaKarlsson-X-jobb/Data/fram_east2ss.txt
```

```
>gmt triangulate D:/LindaKarlsson-X-jobb/Data/fram_east2ss.txt -R-509000.0/397000.0/-1439000.0/-923000.0 -I[nr] -GD:/LindaKarlsson-X-jobb/Data/fram_[nr]_tri_he1ss.nc
```

#### 2.3 Block median

```
>gmt blockmedian D:/LindaKarlsson-X-jobb/Data/fram_west.txt -R-509000.0/397000.0/-1439000.0/-923000.0 -I[nr] > D:/LindaKarlsson-X-jobb/Data/fram_median_[nr].txt
```

```
>gmt surface D:\LindaKarlsson-X-jobb\Data\fram_median_[nr].txt -R-509000.0/397000.0/-  
1439000.0/-923000.0 -I[nr] -GD:\LindaKarlsson-X-jobb\Data\fram_medi_ll[nr]grd.nc -LI-6062.0 -  
Lu1699.03
```

## 2.4 Source files

AGAVE07\_YERMAK\_200m.xyz  
ARK\_xv2.xyz  
ark03\_2\_IBCAO\_PS\_100m\_unedited\_newregion.xyz  
ark04\_3\_IBCAO\_PS\_100m\_unedited\_newregion.xyz  
ark08\_3\_IBCAO\_PS\_100m\_edited\_946\_11.txt  
ark11\_2\_IBCAO\_PS\_100m\_unedited\_newregion.xyz  
ark13\_2\_IBCAO\_PS\_100m\_unedited\_newregion.xyz  
ark13\_3\_IBCAO\_PS\_100m\_unedited\_newregion.xyz  
ark15\_2\_IBCAO\_PS\_100m\_unedited\_newregion.xyz  
ark16\_1\_IBCAO\_PS\_100m\_unedited\_newregion.xyz  
ark17\_1\_IBCAO\_PS\_100m\_unedited\_newregion.xyz  
ark18\_1\_IBCAO\_PS\_100m\_unedited\_newregion.xyz  
ark19\_4a\_IBCAO\_PS\_100m\_unedited\_newregion.xyz  
ark20\_2\_IBCAO\_PS\_100m\_unedited\_newregion.xyz  
ark20\_3\_IBCAO\_PS\_100m\_edited.xyz  
ark22\_1\_IBCAO\_PS\_100m\_unedited\_newregion.xyz  
ark24\_3\_IBCAO\_PS\_100m\_unedited\_newregion.xyz  
ark27\_1\_IBCAO\_PS\_100m\_unedited\_newregion.xyz  
ark27\_2\_IBCAO\_PS\_100m\_unedited\_newregion.xyz  
ARK-III\_3\_wgs84\_IBCAO\_75N\_250m.xyz  
ARK-III\_4\_wgs84\_IBCAO\_75N\_250m.xyz  
ARK-IV\_1\_wgs84\_IBCAO\_75N\_250m.xyz  
ARK-IV\_3\_wgs84\_IBCAO\_75N\_250m.xyz  
ARK-VII\_3\_wgs84\_IBCAO\_75N\_250m.xyz  
ARK-X\_1\_wgs84\_IBCAO\_75N\_250m.xyz  
ARK-XI\_2\_wgs84\_IBCAO\_75N\_250m.xyz  
ARK-XIII\_3\_wgs84\_IBCAO\_75N\_250m.xyz  
ARK-XV\_2\_wgs84\_IBCAO\_75N\_250m.xyz  
ARK-XVI\_1\_wgs84\_IBCAO\_75N\_250m.xyz  
ARK-XVIII\_2\_wgs84\_IBCAO\_75N\_250m.xyz  
ARK-XX\_2\_wgs84\_IBCAO\_75N\_250m.xyz  
ARK-XX\_3\_wgs84\_IBCAO\_75N\_250m.xyz  
ARK-XXII\_1\_wgs84\_IBCAO\_75N\_250m.xyz  
ARK-XXII\_3\_wgs84\_IBCAO\_75N\_250m.xyz  
barents2013.xyz  
BedMachineGreenland-2018-08-28\_bed.txt  
EAGER2011\_100m\_C.xyz  
echo\_general\_greenland.xyz  
echo\_general\_norway.xyz  
EGLACOM\_SVAIS\_2007\_2008\_200m.xyz  
emod\_2018.xyz  
ENC\_soundings\_norway.xyz

GMRT\_E0S128\_320.xyz  
GMRT\_E192S128\_320.xyz  
GRD\_SUPPORT\_11.txt  
GRD\_SUPPORT800.txt  
HDNO.txt  
HH12-50m-UTM.xyz  
HH13-SF-50m-UTM.xyz  
HH14-SF-50m-UTM.xyz  
HLY0503\_YM1\_SWA\_100m.xyz  
HLY0503\_YM2\_SWA\_100m.xyz  
HLY0503\_YM3\_SWA\_100m.xyz  
JCR\_211\_500m.xyz  
JM09H\_2009\_200m.txt  
JM09H\_2010\_200m.txt  
JR142\_200m.txt  
KAN1991.xyz  
KANUMAS1994.xyz  
Knipovich\_200m.txt  
LOMROG07\_EGR\_200m.xyz  
LOMROG07\_MH\_200m.xyz  
LOMROG07\_YP\_200m.xyz  
LOMROG09\_all\_PS75N.xyz  
LOMROG12\_Transit5\_100m\_IBCAO\_75N.xyz  
MSM31\_2013\_200m.xyz  
NEG08.xyz  
NEGC\_2008\_Sites\_100m.xyz  
NEGC\_2008\_Transit\_200m.xyz  
NO2B0878.xyz  
NO2B1076.xyz  
NO2B1078\_ed.xyz  
NO2B1080.xyz  
NO2B1276.xyz  
NO2B1278.xyz  
NO2B1280.xyz  
NO2B1476.xyz  
NO2B1478.xyz  
NO2B1480.xyz  
NO2B1676.xyz  
NO2B1678.xyz  
NO2B1680.xyz  
NO2B1878.xyz  
NO2B1880.xyz  
NorwegianSea\_DTM\_MARUM\_HE449\_Central.xyz  
NorwegianSea\_DTM\_MARUM\_HE449\_North.xyz  
NorwegianSea\_DTM\_MARUM\_HE449\_South.xyz  
NorwegianSea\_DTM\_MARUM\_HE450\_North.xyz

NorwegianSea\_DTM\_MARUM\_HE450\_South.xyz  
norwey\_echo.xyz  
NRL\_BKS\_20090205.txt  
ODEN\_SAT08\_100m\_FShect2.xyz  
ODEN\_SAT0809\_FS02\_100m.xyz  
ODEN\_SAT0809\_FS03\_100m.xyz  
ODEN\_SAT0809\_FS08\_100m.xyz  
ODEN\_SAT0809\_FS09\_100m.xyz  
oden2001.xyz  
OLEX\_0-30E\_75-90N\_PS75N.xyz  
Olex\_IBCAO\_2019\_450m.xyz  
ps85\_IBCAO\_PS\_100m\_edited.xyz  
ps86\_IBCAO\_PS\_100m\_unedited\_newregion.xyz  
ps87\_IBCAO\_PS\_100m\_edited\_940\_17.txt  
ps92\_IBCAO\_PS\_100m\_unedited\_newregion.xyz  
PS93\_1\_IBCAO\_PS\_100m\_unedited\_newregion.xyz  
S0\_DTM50.xyz  
SABVABAA\_SingleBeam\_2011.xyz  
USSUB\_1958\_1982\_orginal\_clean.xyz  
XIX\_4b\_Part1\_wgs84\_IBCAO\_75N\_250m.xyz  
XIX\_4b\_Part2\_wgs84\_IBCAO\_75N\_250m.xyz  
XVII\_1\_Part1\_wgs84\_IBCAO\_75N\_250m.xyz  
XVII\_1\_Part2\_wgs84\_IBCAO\_75N\_250m.xyz  
XVIII\_1\_Part1\_wgs84\_IBCAO\_75N\_250m.xyz